PAPER

High-throughput realization of an infrared selective absorber/emitter by DUV microsphere projection lithography

To cite this article: Alireza Bonakdar *et al* 2016 *Nanotechnology* **27** 035301

IOP Publishing Nanotechnology
Nanotechnology 27 (2016) 035301 (6pp) doi:10.1088/0957-4484/27/3/035301

High-throughput realization of an infrared selective absorber/emitter by DUV microsphere projection lithography

Alireza Bonakdar, Mohsen Rezaei, Eric Dexheimer and Hooman Mohseni

Bio-inspired Sensors and Optoelectronics Laboratory (BISOL), Department of Electrical Engineering and Computer Science, Northwestern University, Evanston, IL 60208, USA

E-mail: hmohseni@northwestern.edu

Received 24 August 2015, revised 26 October 2015
Accepted for publication 17 November 2015
Published 9 December 2015

Abstract

In this paper, we present a low-cost and high-throughput nanofabrication method to realize metasurfaces that have selective absorption/emission in the mid-infrared region of the electromagnetic spectrum. We have developed DUV projection lithography to produce arbitrary patterns with sub-80 nm feature sizes. As examples of practical applications, we experimentally demonstrate structures with single and double spectral absorption/emission features, and in close agreement with numerical simulation. The fundamental mechanism of perfect absorption is discussed as well. Selective infrared absorbers/emitters are critical elements in realizing efficient thermophotovoltaic cells and high-performance biosensors.

Keywords: microsphere photolithography, perfect absorber, thermo-photovoltaic cells, infrared selective absorber/emitter, metasurfaces, nanofabrication

(Some figures may appear in colour only in the online journal)

1. Introduction

An ideal blackbody can perfectly absorb and radiate electromagnetic energy in all directions and polarizations with a broadband power spectrum that follows Planck's law of blackbody radiation. By engineering the blackbody radiation both in spatial and spectral domains [6], an infrared selective absorber/emitter can be realized with significant impact on optical and optoelectronic applications. For example, the detection sensitivity of chemical species significantly increases by utilizing narrowband thermal absorbers in infrared spectroscopy [13]. In thermophotovoltaic technology the conversion efficiency to electricity from a thermal source with blackbody spectrum has an upper limit governed by the detailed balance theory [21]. In contrast, a thermal emitter with narrow power spectrum matched to the bandgap of a photovoltaic cell [15] can exhibit an energy conversion efficiency beyond the detailed balance limit, ideally only limited by the Carnot engine efficiency [25]. Such a thermal emitter can be considered as a passive infrared source [7], where a blackbody source is integrated with a spectral filter that blocks transmission of light, except in a narrow region where the emission is desirable. Unlike the epitaxial grown infrared sources such as interband and intersubband LEDs and lasers [9, 19], the spectral response of the passive infrared sources are tuned geometrically and are not limited by the semiconductor's interband and intersubband energy bandgap [23] providing access to a wide range of spectrum from THz to optical region [7, 15]. Despite these useful applications, a practical realization of infrared selective absorbers/emitters is yet a bottleneck as e-beam lithography is the main fabrication method. Low-cost, large-area, and high-throughput nanomanufacturing methods are now highly sought-after for many applications, including energy harvesting and sensing. Unfortunately, general-purpose nanofabrication tools, such as e-beam lithography and focused ion beam milling, cannot meet these demands [14].

In this paper, we utilize a recently developed fabrication method [1]—DUV microsphere projection lithography—to demonstrate selective emitters/absorbers metasurfaces operating in the mid-infrared region of the spectrum. The proposed nanofabrication method is based on microsphere

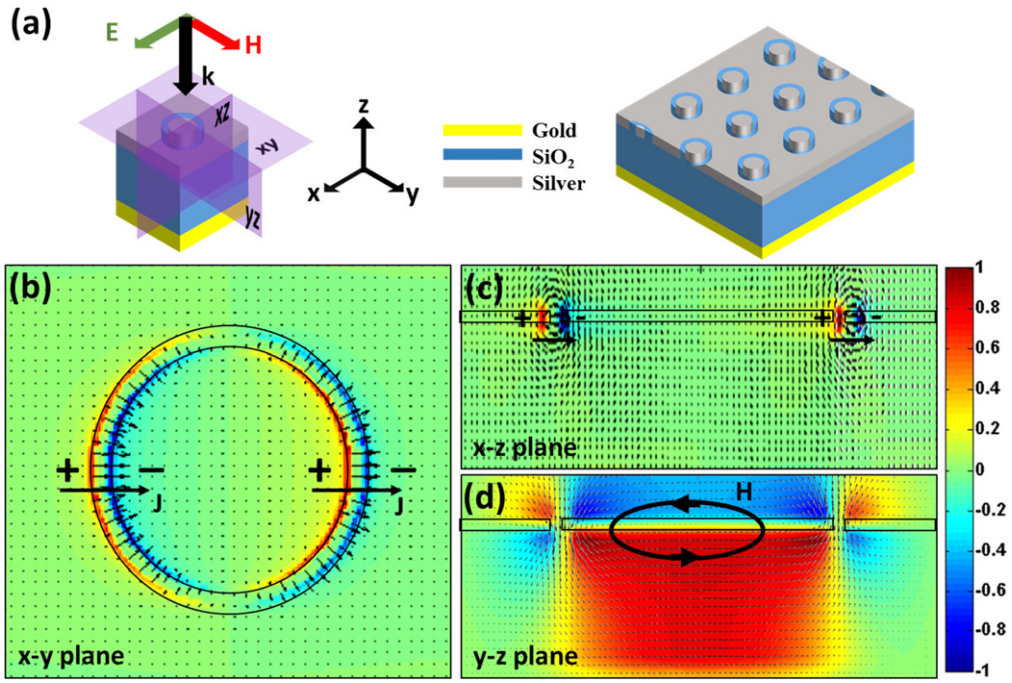

Figure 1. Perfect absorption mechanism. (a) Schematic of an absorber with metasurface composed of hole ring. A unit cell of such an absorber is shown with the direction of incident light and polarization and definition of several planes. (b) Map of polarization charge and displacement current at the *x*–*y* plane passing the metasurface. A net polarization charge and displacement current are produced along the *x*-direction. (c) Map of charge and current in the *x*–*z* plane cutting the structure at the center. (d) Map of the magnetic field along the *y*–*z* plane showing strong enhancement of magnetic field component of incident optical field. The superimposed vector plot shows the magnetic field direction that creates a loop around the displacement current along the *x*-axis demonstrating strong coupling between magnetic and electric field resonances. All simulations are performed using the FDTD method.

photolithography [26], which has been demonstrated as uniquely low-cost, high-throughput and compatible with energy harvesting [8, 16] and sensing [4, 5] material system and processes. Unlike standard microlenses that are produced via a multi-step microfabrication process, microspheres can be fabricated through chemical and physical processes [24]. Convective self-assembly [11], Langmuir-Blodgett technique [20] and Spin-coating [10] are among the promising techniques for rapid coverage of closed packed hexagonal crystals of microspheres in wafer scale. Moreover, separate phases of microsphere synthesization and deposition from nanolithography allows us utilize a variety of substrate materials (metallic/dielectric, organic/inorganic semiconductor, flexible/rigid, and conductive/isolating). In addition, the fabrication area is only limited by the source coverage. In the nanolithography step, microsphere photolithography only requires single flood exposure per sample to produce arbitrary pattern in contrast to scanning based lithography techniques such as electron beam lithography which are highly dependent on area for writing time [22]. In addition, we have shown feature sizes below sub-80 nm [2], which making this DUV lithography method very versatile for realizing optical structures with variety of resonant lengths. In next section, we discuss the mechanism underlying the nearly perfect and narrowband absorption, which based on reciprocity corresponds to efficient selective emission. Next, the proposed fabrication process is presented in details followed by experimental demonstration of nearly perfect absorbers that are realized by DUV microsphere projection lithography.

2. Mechanism of nearly perfect absorption

The concept and design of selective thermal absorbers/emitters have been well developed and their research prototypes are demonstrated based on the optical structures such as the dielectric [18] and metallic [3] photonic crystals, metamaterials [17], and metasurfaces [25]. In this paper, the fabricated absorbers/emitters consists of a metasurface with a dielectric spacer that separates it from a metallic thin film as a ground plate as shown in figure 1(a). The ground plate prevents light from transmission and increases the absorption by reflecting light back to the metasurface. Based on the reciprocity theorem, emissivity is equal to absorbance. Thus, engineering the emissivity is translated into tailoring the absorption spectrum. The absorption spectrum can be controlled by the thickness of spacer, the periodicity of metasurface, and resonance length of meta-atoms. The underlying mechanism of nearly perfect absorption is in tailoring the effective refractive index produced by metasurface. At the resonance peak of absorption, the effective refractive index has a value to match the impedance of the metasurface to the impedance of vacuum, resulting in nearly zero reflection while the imaginary part of the effective index becomes large enough to produce a nearly unity absorption [12]. Tailoring

the effective refractive index requires exciting both electric and magnetic resonances simultaneously, resulting in a strong coupling between the two resonances. For further elaboration, we simulated the electromagnetic interaction with a perfect absorber using FDTD simulation as illustrated in figure 1. To show the strong coupling between the electric and magnetic resonances, we mapped the polarization charges and displacement current vectors in figures 1(b) and (c) at the resonance where absorption is maximum. In both figures, polarization charges accumulated at the edge of the top metal, producing a net electric dipole on both sides of the ring. The displacement current is shown in vectors, pointing from positive to negative charges, producing a net current along the polarization direction (*x*-direction). The displacement current in the *x*-direction, in turn, produces a magnetic field along the magnetic field component of the incident light in the *y*-direction. Figure 1(d) shows the map of the magnetic field along the y direction, as well as a vector plot illustration of magnetic field with its circular nature. The circulation of the magnetic field around the displacement current reveals a strong coupling between the electric and magnetic resonances at absorption peak. Note that the ground plate produces an image of the polarized charge and displacement current with opposite polarity and direction, respectively. The antiparallel currents at the metasurface and inside the ground plate (imaged one) produces an effective current loop. As a results, the unusual extension of the magnetic field toward the ground plate in figure 1(d) is the consequence of the antiparallel currents that produces magnetic field in the dielectric spacer.

3. Nanofabrication procedure using DUV microsphere lithography

Figures 2(a), (b) and (c) show the top-view SEM images of the fabricated absorbers with meta-atoms in the form of a circle, ring and crescent openings, respectively. The defects in fabricated samples are mainly due to the microsphere size and imperfection in sphere deposition. Using spheres with high uniformity and reducing deposition speed can reduce these defects. As we show in next section, defects only broaden the optical response and reduce the resonance peak magnitude, resulting in fair dimensional tolerance for optical response for applications such as solar cells. The fabrication procedure is sketched in figure 2(d). A silicon wafer is cleaned via RCA cleaning steps. Then, a 100 nm thick gold is deposited on the sample using e-beam evaporation. A 5 nm thick titanium is deposited beforehand as an adhesion agent. Next, a 300 nm thick SiO_2 is deposited by PECVD. The thickness accuracy is confirmed by Elipsometry measurement. A 280 nm thick ma-N 2403 DUV photoresist (MicroChem) is spun at 6000 rpm for 30 s onto the wafer, followed by soft-baking of the sample in an oven at 90 °C for 3 h. The next step is DUV lithography to produce high aspect-ratio photoresist pillars. The details of the DUV microsphere projection lithography are documented elsewhere [1]. In brief, a monolayer of microspheres with 2 μm diameter (microParticles GmbH with 2.5% standard deviation) is deposited on a $\sim$1 cm^2 area of the wafer. During

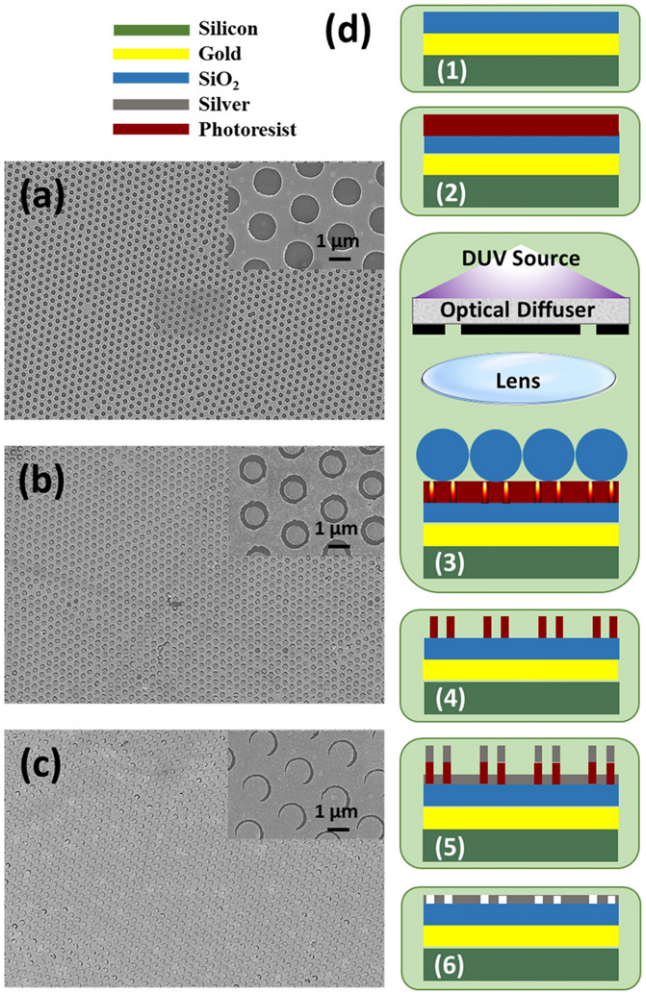

Figure 2. Top-view SEM images of the fabricated absorbers with meta-atoms in the form of (a) circle, (b) ring and (c) crescent openings. Note that defects in fabricated samples are mainly caused by microsphere size and arrangement variations during microsphere deposition. Using spheres with high uniformity and deposition at low speed can reduce defects. (d) Fabrication process: (1) deposition of gold and SiO_2 by e-beam evaporation and PECVD, respectively. (2) Spinning DUV photoresist and soft-baking the sample in the oven. (3) DUV microsphere projection lithography. (4) Cold-developing to produce photoresist pillars with ring and crescent patterns. (5) Deposition of silver by e-beam evaporation. Note that optical structure and microspheres are not drawn in the real scale. (6) Lift-off of photoresist by dipping the sample into acetone with ultra-sonication treatment.

exposure to the DUV source, an objective lens projects a mask pattern on the array of microspheres. In order to increase the quality of imaging and uniformity, a fused silica optical diffuser is placed between the DUV source and the mask. The mask and sample are placed at the front and back focal points of the objective lens, respectively. Each microsphere images the mask pattern onto the photoresist. Then, the microspheres are removed from the sample by an ultra-sonication bath for 30 s. In order to increase the contrast to the pattern, the sample is developed in ma-D 525 (MicroChem) at -4 °C for 2 min. A cold plate is used to control and stabilize the temperature of develop solution with a precision of 1 °C.

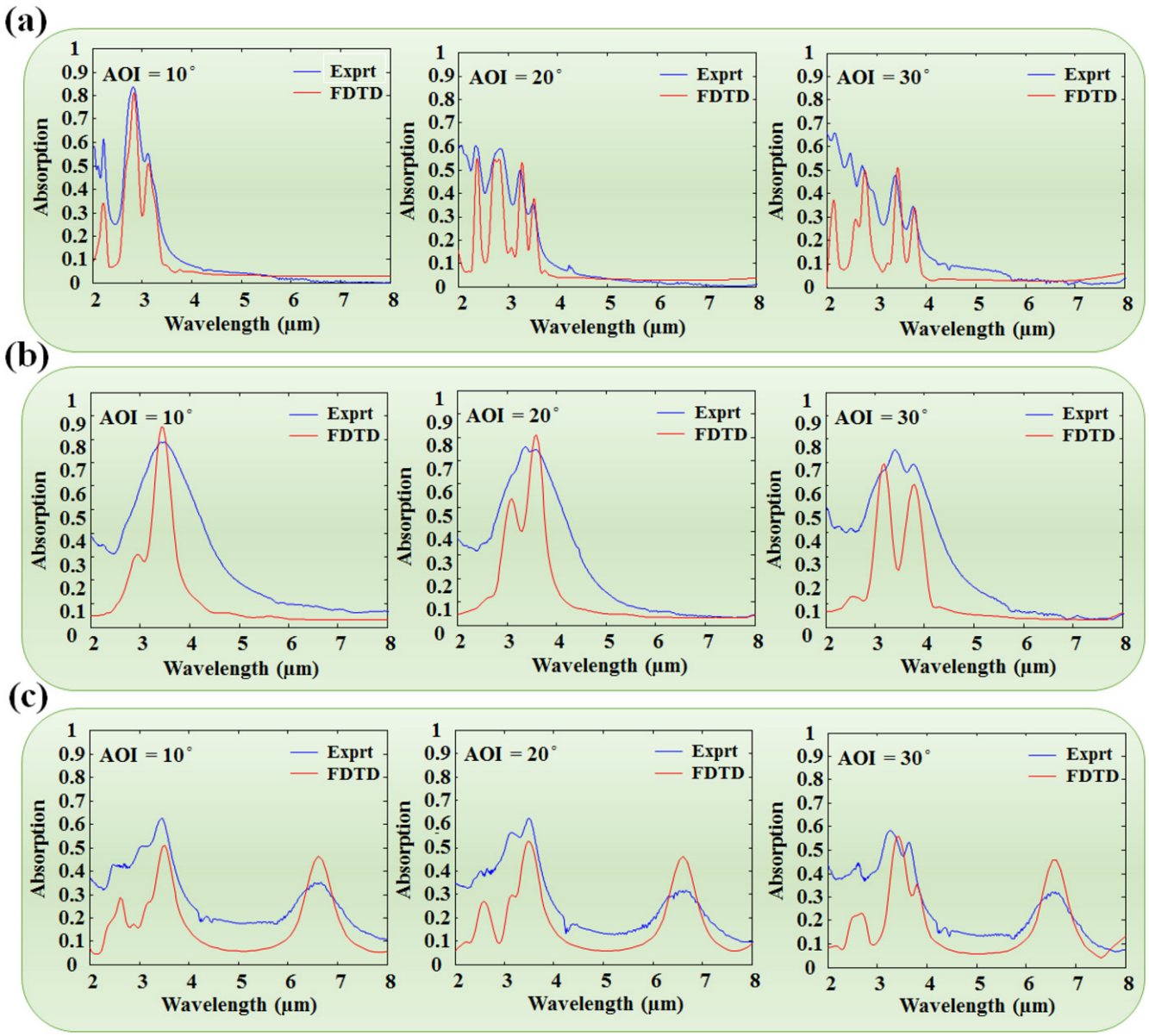

Figure 3. Comparing the measured absorption spectrum by FTIR and simulated by FDTD (a) for a circular meta-atom, (b) for a full ring meta-atom, and (c) for a crescent (broken ring) meta-atom. Since, the FTIR source in the measured signal is un-polarized, the simulated spectra are derived from averaging the two spectra of the linear polarization sources. Since the response is polarization dependent, the average absorption reduces from nearly unity value. The measured signal is normalized by a gold coated mirror as a reference. The high absorption below 2.5 μm is artificial as the responsivity of MCT detector deteriorates below 2.5 μm. The extra broadening in the measurement is due to poly-crystal arrangement of metasurfaces and non-plane wave incident source.

A 30 nm silver coating is deposited on the developed pattern by e-beam evaporation. Finally, the lift-off is completed by dipping the sample into acetone while treating it in an ultra-sonication bath for 30 min. High aspect ratio features of the ring and crescent nanopillars are crucial for successful, single-step lift-off process.

4. Results and discussion

We demonstrated narrowband perfect absorption using Fourier transform infrared spectroscopy (FTIR) to measure the specular reflection at different angles of incidence (AOI). In addition, we confirmed the experimental results with full-wave FDTD simulations. Figure 3 shows the measured absorption spectrum and the corresponding simulated results. Since the ground metal is optically thick enough to ignore any transmission, the absorption spectrum of the samples can be directly resolved by measuring the reflection spectrum. In order to eliminate FTIR and source frequency responses in the final results, we used a thick gold plate as a reference sample to ratio the measured spectra of the samples. A liquid nitrogen-cooled MCT detector is used to detect the reflected light from the sample. Since the source is un-polarized in the experiment, measurement results do not show perfect absorption as absorption is less than 100%. Similarly, in

simulation, we averaged the reflected spectra of the two simulations with their source are plane-wave with linear in-plane polarization states. The lateral boundary conditions are defined as Bloch boundary conditions to simulate an infinite hexagonal array of meta-atoms. The perpendicular boundary conditions are assumed to be perfectly matched layers in the air and metallic in the ground plate. All geometrical dimensions are extracted from SEM images in the insets of the measured spectra in figure 3. Comparing both measured and simulated results shows well-matched spectra, and confirmed the perfect absorption feature of the fabricated samples using deep UV microsphere projection lithography. An extra broadening that is observed in the measured spectra is due to size deviation of meta-atoms, non-plane-wave sources of incidence, and the polycrystalline configuration of the metasurface compared with the monocrystalline array in the simulation. Nevertheless, the resonance peak of absorption is strong enough to be resolved.

Note that in our experiment, all samples have the same geometrical and material properties except for their meta-atom shape. Therefore, comparing these three difference meta-atoms reveals several interesting conclusions. First, the absorption spectrum of the circular meta-atoms in figure 3(a) show the highest sensitivity to the AOI. Another interesting phenomenon is the absorption peak around 6.6 μm wavelength in crescent as a broken ring in figure 3(c), which does not exist in a full symmetric ring in figure 3(b). The main difference between the two meta-atoms are the presence of a capacitor at the gap between two ends of the crescent that can add another pole to the reflection response of the absorber. Additional pole adds another resonance in the spectrum. Finally, the absorption spectrum of the crescent is highly sensitive to the polarization of incident light due to its asymmetric structure. Therefore, by averaging two polarizations, the absorption peak reduces around 50% compared with symmetric full ring and circular meta-atoms.

5. Conclusion

In conclusion, we have realized selective absorbers operating in the mid-infrared region of the spectrum. The fabrication method is DUV microsphere projection lithography, which is uniquely low-cost, high-throughput and compatible with large area nano-manufacturing of energy harvesting and sensing applications. The structure of selective absorbers consists of a metallic thin film as a ground plate with a dielectric spacer that separates it from a metasurface. We have demonstrated nearly perfect absorption and narrowband bandwidth using FTIR reflection measurement and confirmed it with FDTD simulations. Since in measurement, we used an unpolarized source, the absorption spectrum is less than 100%. To have simulation results with a close match to the experiment, we have averaged the absorption spectrum of the two orthogonal polarization states. The absorption band is highly controllable over a wide range of the spectrum, merely by tailoring the resonance length of the optical scatterers.

Acknowledgments

The authors would like to acknowledge partial support from NSF award # ECCS-1310620, ARO award # W911NF-13-1-0485 and W911NF-11-1-0390. This work utilized Northwestern University Micro/Nano Fabrication Facility (NUFAB), which is supported by the State of Illinois and Northwestern University and High Performance Computational Center (QUEST) at Northwestern University.

References

[1] Bonakdar M R A, Brown R L, Fathipour V, Dexheimer E, Jang S J and Mohseni H 2015 Deep UV microsphere projection lithography *Opt. Lett.* **40** 2537
[2] Bonakdar A, Jang S J, Brown R L, Rezaei M and Mohseni H 2014 *Proc. SPIE* **9170** 917016
[3] Celanovic I, Jovanovic N and Kassakian J 2008 Two-dimensional tungsten photonic crystals as selective thermal emitters *Appl. Phys. Lett.* **92** 193101
[4] Chang Y-C, Chung H-C, Lu S-C and Guo T-F 2013 A large-scale sub-100 nm Au nanodisk array fabricated using nanospherical-lens lithography: a low-cost localized surface plasmon resonance sensor *Nanotechnology* **24** 095302
[5] Chang Y-C, Wang S-M, Chung H-C, Tseng C-B and Chang S-H 2012 Observation of absorption-dominated bonding dark plasmon mode from metal–insulator–metal nanodisk arrays fabricated by nanospherical-lens lithography *ACS Nano* **6** 3390–6
[6] De Zoysa M, Asano T, Mochizuki K, Oskooi A, Inoue T and Noda S 2012 Conversion of broadband to narrowband thermal emission through energy recycling *Nat. Photonics* **6** 535–9
[7] Diem M, Koschny T and Soukoulis C M 2009 Wide-angle perfect absorber/thermal emitter in the terahertz regime *Phys. Rev.* B **79** 033101
[8] Dong P *et al* 2013 282 nm AlGaN-based deep ultraviolet light-emitting diodes with improved performance on nano-patterned sapphire substrates *Appl. Phys. Lett.* **102** 241113
[9] Godard A 2007 Infrared (2–12 μm) solid-state laser sources: a review *C. R Phys.* **8** 1100–28
[10] Jiang P and McFarland M J 2004 Large-scale fabrication of Wafer-Size colloidal crystals, macroporous polymers and nanocomposites by spin-coating *J. Am. Chem. Soc.* **126** 13778–86
[11] Kumnorkaew P, Ee Y-K, Tansu N and Gilchrist J F 2008 Investigation of the deposition of microsphere monolayers for fabrication of microlens arrays *Langmuir* **24** 12150–7
[12] Landy N I, Sajuyigbe S, Mock J J, Smith D R and Padilla W J 2008 Perfect metamaterial absorber *Phys. Rev. Lett.* **100** 207402
[13] Li Y, Su L, Shou C, Yu C, Deng J and Fang Y 2013 Surface-enhanced molecular spectroscopy (SEMS) based on perfect-absorber metamaterials in the mid-infrared *Sci. Rep.* **3** 2865
[14] Liu Q, Duan X and Peng C 2014 *Novel Optical Technologies for Nanofabrication* (Berlin: Springer)
[15] Liu X, Tyler T, Starr T, Starr A F, Jokerst N M and Padilla W J 2011 Taming the blackbody with infrared metamaterials as selective thermal emitters *Phys. Rev. Lett.* **107** 045901
[16] Liyanage W P R, Wilson J S, Kinzel E C, Durant B K and Nath M 2015 Fabrication of CdTe nanorod arrays over large area through patterned electrodeposition for efficient

solar energy conversion *Sol. Energy Mater. Sol. Cells* **133** 260–7
[17] Ogawa S, Fujisawa D, Hata H, Uetsuki M, Misaki K and Kimata M 2015 Mushroom plasmonic metamaterial infrared absorbers *Appl. Phys. Lett.* **106** 041105
[18] Oskooi A, Favuzzi P A, Tanaka Y, Shigeta H, Kawakami Y and Noda S 2012 Partially disordered photonic-crystal thin films for enhanced and robust photovoltaics *Appl. Phys. Lett.* **100** 181110
[19] Schubert E F and Kim J K 2005 Solid-state light sources getting smart *Science* **308** 1274–8
[20] Shimmin R G, DiMauro A J and Braun P V 2006 Slow vertical deposition of colloidal crystals: a Langmuir–Blodgett process? *Langmuir* **22** 6507–13
[21] Shockley W and Queisser H J 1961 Detailed balance limit of efficiency of p–n junction solar cells *J. Appl. Phys.* **32** 510–9
[22] Smith J H, Crosland N, Doran S, Dowling R C, Hartley J G, Hoyle P C, King D M, Kutcher L, McClelland A and Turnidge M 2014 *Proc. SPIE* **9049** 90490O
[23] Sorokina I T and Vodopyanov K L 2003 *Solid-State Mid-Infrared Laser Sources* vol 89 (Berlin: Springer)
[24] Stöber W, Fink A and Bohn E 1968 Controlled growth of monodisperse silica spheres in the micron size range *J. Colloid Interface Sci.* **26** 62–9
[25] Woolf D, Hensley J, Cederberg J G, Bethke D T, Grine A D and Shaner E A 2014 Heterogeneous metasurface for high temperature selective emission *Appl. Phys. Lett.* **105** 081110
[26] Wu W, Katsnelson A, Memis O G and Mohseni H 2007 A deep sub-wavelength process for the formation of highly uniform arrays of nanoholes and nanopillars *Nanotechnology* **18** 485302